Non-electronic gas sensor from electrospun mats of liquid crystal core fibers for detecting volatile organic compounds at room temperature: *Supplemental Online Material*

Catherine G. Reyes, Anshul Sharma and Jan P.F. Lagerwall

July 18, 2016

S1 Complete description of experimental details

S1.1 Coaxial spinneret and collection geometries

For constructing the coaxial spinneret, a thin flexible silica capillary (www.bgb-shop.com, Part #: TSP-250350; inner diameter, ID: 250 μm, outer diameter, OD: 360 μm), which will transport the LC, is inserted throughout the long axis of a polypropylene Reducing T-coupler (Carl Roth; ID: 3.2 mm for longitudinal openings, 1.6 mm for the lateral), see Figure S1A. One end of the capillary emerges from the T-coupler into a short piece of stainless steel tubing (Unimed, Lausanne, Switzerland; ID: 0.70 mm, OD: 1.10 mm, length: 50 mm) such that the capillary is positioned coaxially inside it. One end of the inner capillary is aligned with the opening of the stainless steel tube, which serves as the high-voltage electrode during spinning. In the other direction, the silica capillary extends some 20 cm away from the T-coupler. To the lateral opening of the T-coupler a polytetrafluoroethylene (PTFE) tube (ID: 0.8 mm, OD: 1 mm) is connected, allowing the polymer solution to be flown into the metal tube. All connections are kept tight and sealed using high-density PTFE tape and shrinking tube.

The other ends of the silica capillary and the teflon tube, respectively, are inserted, via septum covers, into vials with 5CB and PVP solution, respectively. The silica capillary punctures the septum directly, whereas the PTFE tube was fitted with an 18 gauge 2" long (18G x 2") bevelled tip syringe needle. The openings of the needle and of the silica capillary are located at the bottom of their respective liquid volume. For each vial an additional short syringe needle is also pierced through the septum, ending above the surface of the contained liquid. These needles are connected, via soft rubber tubing, to the Fluigent MFCS unit.

To start the electrospinning process the two vials are pressurized by the MFCS unit, initiating flow of the polymer solution and 5CB through their respective tubing into the coaxial spinneret. Both liquids converge for coaxial spinning at the metal capillary end,

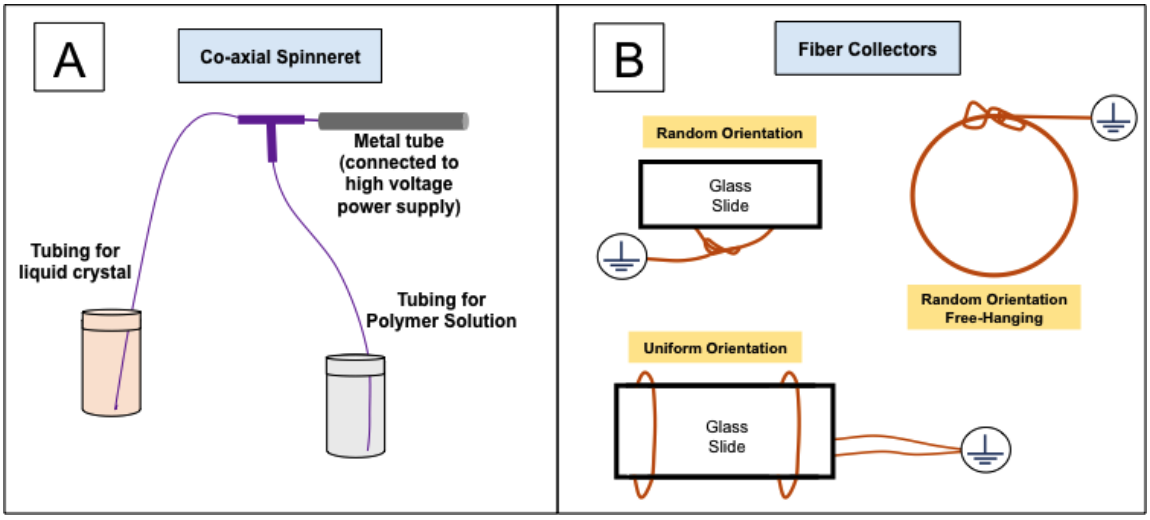

Figure S1: Schematic of coaxial electrospinning spinneret (A) and fiber collectors (B).

5CB being ejected into the externally flowing PVP solution. The PVP solution was always flown at a rate of 0.9 mL/h, whereas the LC was flown at 0.50 mL/h as standard, and 1.5 mL/h as elevated flow rate.

When an electric field of adequate strength (ranging from 7 - 10 kV) was applied between spinneret and the grounded collector electrode a composite Taylor cone developed, from which the jet is ejected, see Figure S2. Due to gravity, the two fluids do not align concentrically in the Taylor cone, but they do in the jet from which the coaxial fibers are formed after evaporation of the solvent.

For collecting fibers on substrates, standard microscopy slides were inserted into a designated holder in the collector. Bare copper wire (approximately 26G, or 0.4 mm in diameter) connected to ground was used as counter electrode during spinning. The wire was fashioned in different ways depending on which type of mat was desired, see Figure S1B. For collecting aligned fibers, two grounded wire loops were placed at each end of the slide, such that fibers extend back and forth, uniformly aligned between the two grounded electrodes [1]. When a random mat on glass was desired, a single copper wire was placed on the back side of the slide. Finally, for collecting free-hanging fibers a single wire loop, aligned with its plane perpendicular to the spinning jet, was used, the fibers extended in random directions across the space defined by the wire loop.

Glass slides (Duran, 76 x 26 mm^2, purchased from Carl Roth), and silica substrates (SPI Supplies, 5 x 7mm, #4137SC-AB) were used to collect the fibers for the gas sensing experiments.

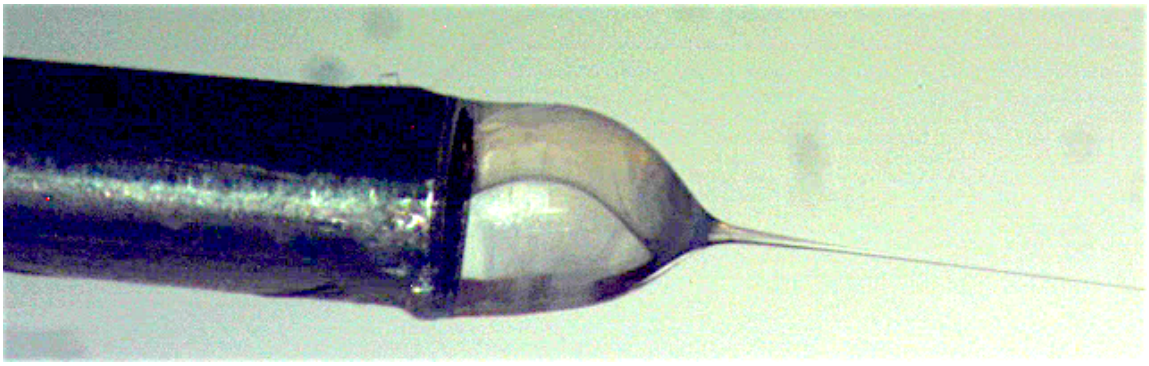

Figure S2: The stainless steel tube functioning as high-voltage electrode and main spinneret (left) with the composite Taylor cone protruding towards the right. The polymer solution collects at the bottom of the Taylor cone due to gravity. On the right the jet that will form the fibers is ejected. Although it is difficult to see from the photo, the jet contains LC inside polymer solution in a coaxial arrangement, ensuring the core-sheath geometry of the final fiber. The picture has been digitally enhanced for clarity of details.

S1.2 Microscopic imaging

The fiber mats were analysed by optical microscopy (POM, Olympus BX51) in polarizing and bright-field contrast, as well as with Scanning Electron Microscopy (SEM, JEOL JSM-6010LA). Prior to SEM imaging the samples were coated with a thin layer of gold (Balzers SCD 050 Sputter Coater; 130 s. sputtering time) to avoid electrical charge build-up.

The software ImageJ (obtained from: https://imagej.nih.gov/ij/) was used to estimate the outer sheath fiber diameters, and the thicknesses of the fiber cores.

S2 Control experiments with PVP fibers without LC

To rule out that the response seen from the LC-filled fibers is in fact due to the PVP making up the sheath, control experiments were carried out in which pure PVP fibers, containing no LC, were exposed to toluene while being observed between crossed polarizers. The result is shown in Figure S3, for a free-hanging mat as well as for mats on substrates, for random fiber orientations as well as for uniformly aligned fibers. In no case does the appearance change as a result of the toluene exposure.

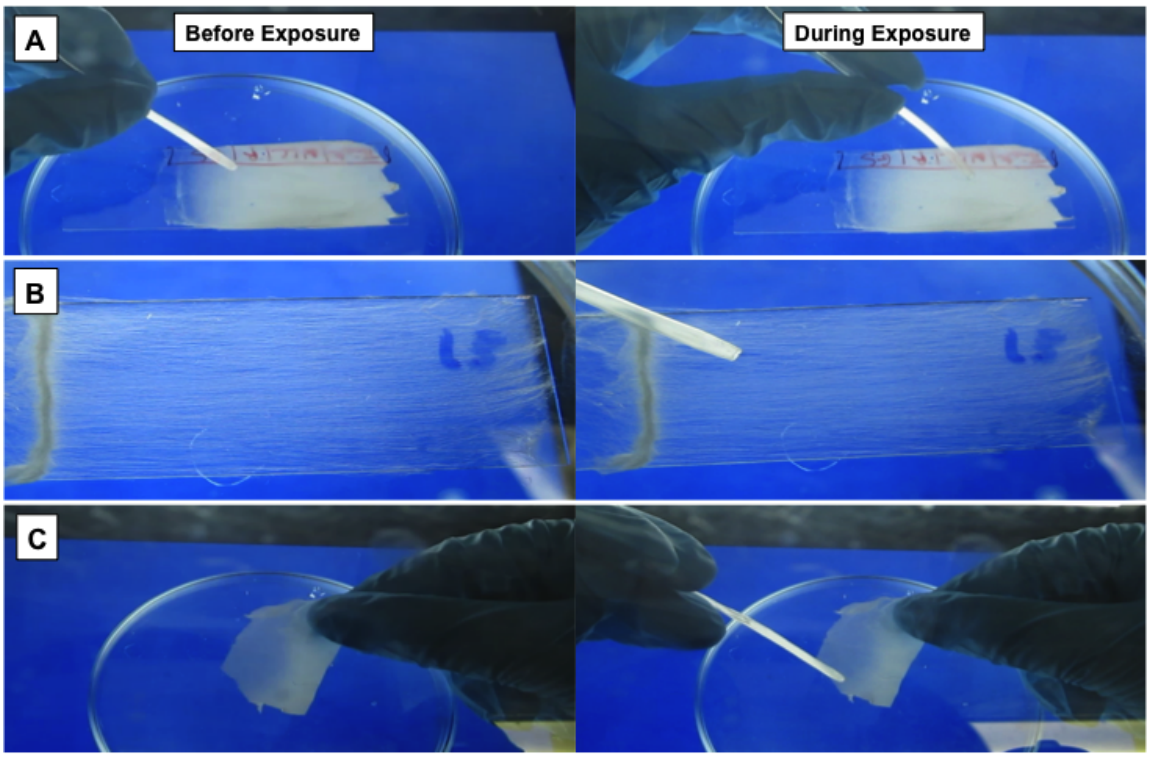

Figure S3: Pure PVP mats (not containing any liquid crystal), held between crossed polarizers, before and during toluene gas exposure. Sample A contains randomly oriented fibers on glass, sample B uniformly aligned fibers on glass, whereas sample C is a free-hanging mat (no substrate) with random fiber orientations.

S3 Upper estimate of toluene concentration during experiments

The equipment used in the present study does not allow us to establish the concentration of toluene to which the fibers are actually exposed, but we can at least set an upper limit to it, since it cannot be higher than the concentration in the atmosphere above the liquid toluene in the reservoir used during the experiment. It should be emphasized that the actual concentration of toluene sensed by the fibers is much lower, but having an upper limit, even if it is grossly overestimated, is still valuable.

According to Goodwin [2] the vapor pressure of toluene at 23°C (the laboratory temperature during our experiments) is 0.034 bar. The atmospheric pressure in the lab was unfortunately not measured during the experiments, but as we are here aiming for a very rough upper estimate, we can simply use standard atmospheric pressure, 1.013 bar, as an estimate of the total pressure in the atmosphere above the liquid toluene. This yields, for the concentration x of toluene:

$$x = \frac{p_{toluene}}{p_{total}} = \frac{0.034}{1.013} \approx 0.03 \tag{1}$$

Thus, we can safely state that the concentration of toluene during the experiments was much lower than 3%.

S4 Estimate of variations in sheath thickness as a function of spinning fluid flow ratios

Consider an infinitesimal segment ΔL of a core-sheath jet, shortly, but not directly, after exiting the Taylor cone (in practice, it should be short enough that we can neglect variations of the core-sheath geometry along the length of the segment). We define it as the length of jet passing a certain point beyond the Taylor cone end during a certain, very small, time Δt. Neglecting the evaporation of the polymer solvent that has taken place so far, we can then state that the flow rate with which we pump the polymer solution is a measure of the amount of polymer solution in the sheath regime of the segment. Moreover, assuming that also differences in elongational viscosity between liquid crystal core fluid and sheath polymer solution are negligible, the length ΔL of the segment should be identical for the core and the sheath. In reality, the non-zero difference in elongational viscosities means that core and sheath will be stretched by different factors, the difference mediated either via slippage between core and sheath fluid or via shear stress within each fluid. In either case, the result is slightly different lengths ΔL_c and ΔL_s for core and sheath, respectively, during the time Δt.

Under these simplifying assumptions, the ratio between the flow rates is directly proportional to the relative areas of core and sheath in the cross section, shown in Figure S4.

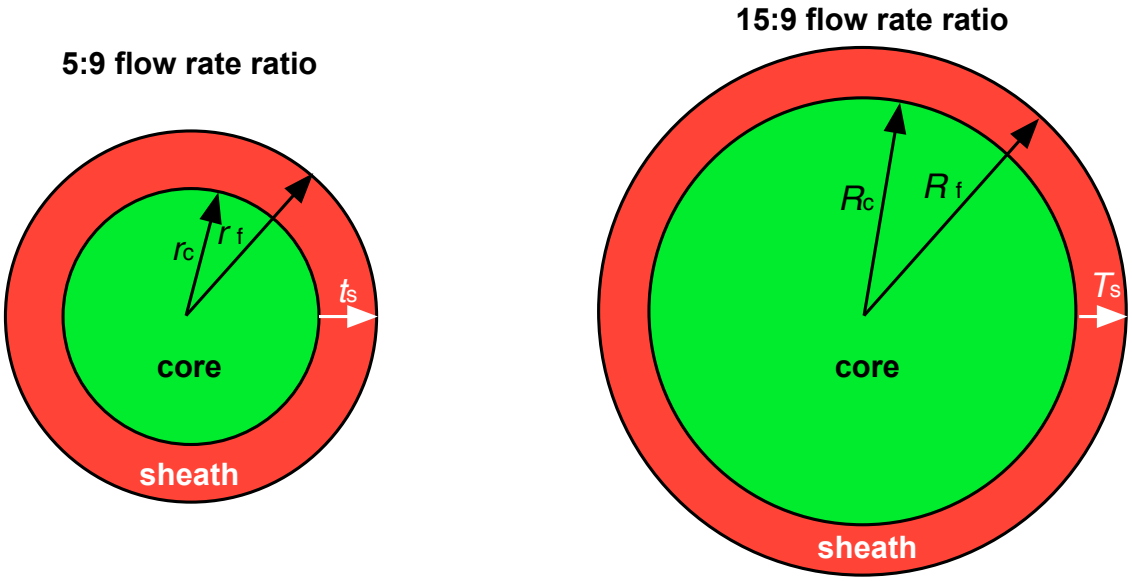

Figure S4: Definitions of parameters of the coaxial fiber cross sections used for obtaining a rough estimate of the effect of flow rate ratio on the final core-sheath area relation.

At 5:9 core:sheath flow rate ratio, the sheath area (red in the figure) should be almost twice as large as the core area (green in the figure). Let the core radius under these conditions be r_c and the total fiber radius be r_f, the sheath thickness thus being $t_s = r_f - r_c$, see the left drawing in Figure S4.

The cross section area of the core is:

$$a_c = \pi r_c^2 \tag{2}$$

and this would be equal to 5/9 of the cross section area a_s of the sheath, or 5/14 of the cross section area a_f of the fiber, thus:

$$a_f = \pi r_f^2 = \frac{14}{5} a_c = 2.8\pi r_c^2 \Rightarrow r_f = \sqrt{2.8} r_c \Rightarrow t_s = (\sqrt{2.8} - 1) r_c \approx 0.67 r_c \tag{3}$$

Now consider the situation with three times higher LC core flow rate but maintained polymer sheath solution flow rate (right drawing in Figure S4). Under the same assumptions, the overall fiber diameter and the core diameter must increase from r_f and r_c to $R_f > r_f$and $R_c > r_c$, respectively, but the sheath thickness must decrease, from t_s to $T_s < t_s$, since the sheath cross section area, being proportional to the polymer solution flow rate, is unchanged. But how much does it decrease? The core area is now:

$$A_c = \pi R_c^2 = 3\pi r_c^2 \Rightarrow R_c = \sqrt{3} r_c \tag{4}$$

The sheath area is unchanged, thus:

$$A_s = a_s = \frac{9}{5}a_c = \frac{9}{5}\pi r_c^2 \Rightarrow A_f = A_s + A_c = (\frac{9}{5} + 3)\pi r_c^2 = \frac{24}{5}\pi r_c^2 \Rightarrow R_f = \sqrt{\frac{24}{5}}r_c \quad (5)$$

The new sheath thickness is then given by:

$$T_s = R_f - R_c = \sqrt{\frac{24}{5}}r_c - \sqrt{3}r_c = (\sqrt{\frac{24}{5}} - \sqrt{3})r_c \approx 0.46r_c \quad (6)$$

which means that the sheath thickness at the 15:9 flow rate ratio would be about 69% of the sheath thickness at 5:9 flow rate ratio.

One must note that the simplifications done for this estimate are rather severe. Solvent evaporation from the polymer solution takes place continuously and the evaporation rate is proportional to the outer surface area of the sheath, thus the solvent will evaporate faster during 15:9 ratio spinning than during 5:9 ratio spinning. On the other hand, ethanol will also diffuse to some extent into the 5CB core, and also this diffusion will be faster during 15:9 ratio spinning due to the larger 5CB-PVP solution interface. However, the ethanol does not stay in the 5CB but will eventually evaporate, passing through the PVP sheath to do so. At later stages during spinning the internal diffusion will thus reverse direction. Moreover, the polymer solution and LC cannot be expected to have identical elongational viscosities, in particular as both in fact vary throughout the spinning process. As the PVP solution loses solvent its viscosity increases, while that of the LC core should decrease somewhat due to the diffusion of ethanol into the core. A more realistic calculation, taking these complex simultaneous phenomena into account (as well as other phenomena that may further influence the result) is dramatically more complicated and outside the scope of this paper. It appears rather clear, however, that the impact of the neglected phenomena would be to further decrease the sheath thickness at increased LC flow rate, thus the 69% figure should be considered a generous upper estimate.

S5 Appearance of cracks in the sheath of fibers spun in humid atmosphere

While no pores could be detected in the sheaths of fibers spun with high humidity or with high LC-to-polymer-solution flow rate, we did notice a few cracks in the fibers spun at elevated humidity, see Figure S5. While each crack could be quite large, improving the access of toluene to the LC core, they were so rare that we do not believe they had any significant influence on the overall response.

S6 Description of video files

1. Response to toluene exposure of fresh sample with uniformly aligned fibers between crossed polarizers, the fibers oriented along the polarizer. The macroscopic response

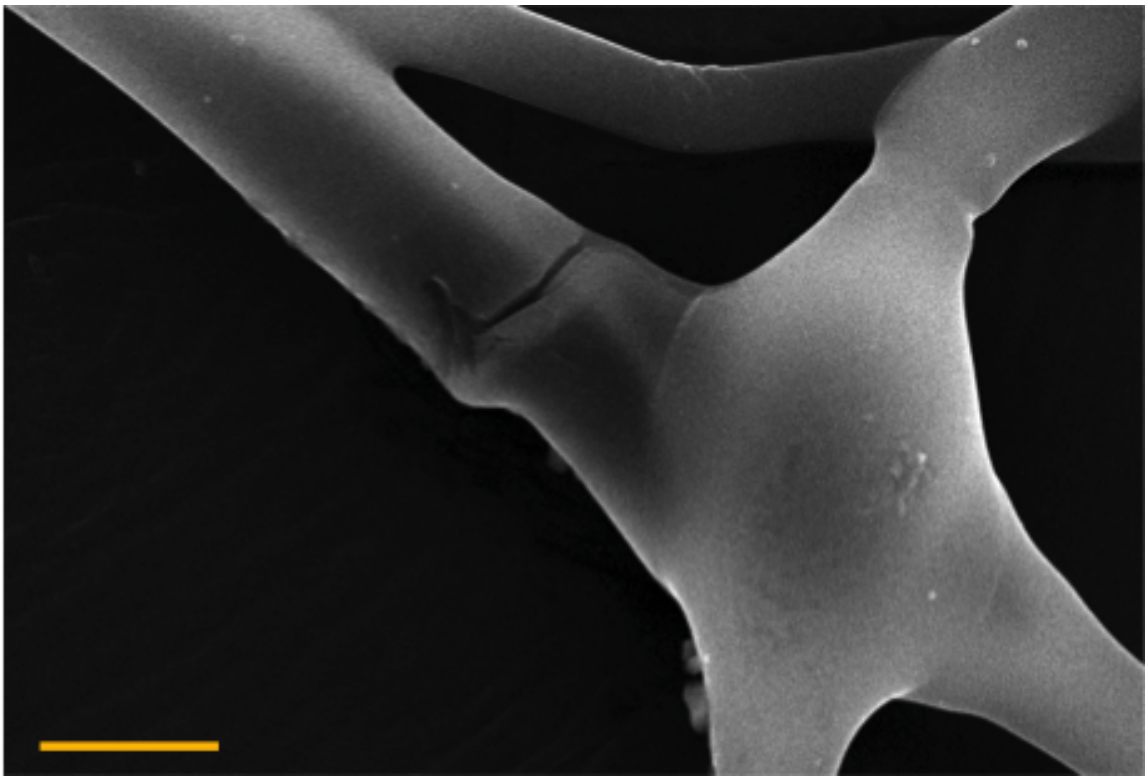

Figure S5: SEM image of an area from the mat spun at high humidity, exhibiting a crack across one fiber. Scale bar is 10 μm.

(complete mat) is followed by the microscopic response (individual fibers).

2. Response to toluene exposure of aged sample with uniformly aligned fibers between crossed polarizers, the fibers oriented along the polarizer.

3. Response to toluene exposure of aged sample with uniformly aligned fibers between crossed polarizers, the fibers oriented 45° to the polarizer. The macroscopic response (complete mat) is followed by the microscopic response (individual fibers).

4. Response to toluene exposure of sample with randomly oriented fibers of uniformly cylindrical morphology, between crossed polarizers. The macroscopic response (complete mat) is followed by the microscopic response (individual fibers).

5. Response to toluene exposure of sample with fibers containing no LC (control experiment).

6. Response to toluene exposure of free-hanging mat with LC-containing fibers, between crossed polarizers.The macroscopic response (complete mat) is followed by the microscopic response (individual fibers). In the latter section many fibers are out of focus since there is no uniform focal plane for the free-hanging mat.

7. Response to toluene exposure of a sample with irregular, beaded, fibers, spun with an LC-to-polymer solution flow rate ratio of 3:1, observed between crossed polarizers.

8. Response to toluene exposure of a sample with irregular, beaded, fibers, spun at high humidity (61%), observed between crossed polarizers. The central area of the mat is too thick for a clear response to be observable; the scattering from the PVP sheath dominates.

9. Response to toluene exposure of a sample with irregular, beaded, fibers, spun with an LC-to-polymer solution flow rate ratio of 3:1, observed without polarizers.

10. Response to toluene exposure of a sample with irregular, beaded, fibers, spun at high humidity (61%), observed without polarizers.

References

[1] D. Li, Y. Wang, and Y. Xia, "Electrospinning of polymeric and ceramic nanofibers as uniaxially aligned arrays," *Nano. Lett.*, vol. 3, no. 8, pp. 1167–1171, 2003.

[2] R. D. Goodwin, "Toluene thermophysical properties from 178 to 800 k at pressures to 1000 bar," *J. Phys. Chem. Ref. Data*, vol. 18, no. 4, pp. 1565–1636, 1989.